Nano Energy (2015) 11, 28–37

Available online at www.sciencedirect.com

ScienceDirect

journal homepage: www.elsevier.com/locate/nanoenergy

RAPID COMMUNICATION

Fabrication of wheat grain textured TiO_2/CuO composite nanofibers for enhanced solar H_2 generation and degradation performance

Liangliang Zhu[a], Minghui Hong[a,b], Ghim Wei Ho[a,b,c,*]

[a]Department of Electrical and Computer Engineering, National University of Singapore, 4 Engineering Drive 3, 117576, Singapore
[b]Engineering Science Programme, National University of Singapore, 9 Engineering Drive 1, 117576, Singapore
[c]Institute of Materials Research and Engineering, A*STAR (Agency for Science, Technology and Research), 3 Research Link, 117602, Singapore

Received 23 July 2014; received in revised form 26 September 2014; accepted 28 September 2014
Available online 27 October 2014

KEYWORDS
Hydrogen;
TiO_2/CuO nanocomposite;
Textured nanofibers;
Photocatalyst

Abstract

We report herein a simple, low-cost and scalable fabrication of unique wheat grain-like textured TiO_2/CuO composite nanofibers (NFs) by electrospinning. Unlike conventional surface coupling/loading of co-catalyst nanoparticles, incorporation of copper nanoparticles during the electrospinning of TiO_2 NFs ensures good stability and recyclability due to resistance against nanoparticles leaching. Optimization of electrospun NFs shows that TiO_2/CuO composite NFs with 2.5 wt% copper nanoparticles, annealed at 500 °C exhibit highly textured structure with enhanced photocatalytic H_2 generation of 16.8 times higher than that of bare TiO_2 NFs. Furthermore, the electrospun TiO_2/CuO composite NFs demonstrate favorable photodegradation activity. The ease of tuning morphology and its heterostructure composite as well as separation and recovery of the fibrous photocatalyst after photoreaction renders immense potential to remedy global environmental and energy issues.

Introduction

Hydrogen (H_2) as a renewable and sustainable form of energy has drawn dramatically increasing attention due to clean emission and high conversion efficiencies [1]. Among many methods including steam reforming [2], electrochemistry [3] and biotechnology [4], the photochemical water

*Corresponding author.
E-mail address: elehgw@nus.edu.sg (G.W. Ho).

http://dx.doi.org/10.1016/j.nanoen.2014.09.032

splitting has been considered as one of the major strategies for hydrogen production [5,6]. Titanium dioxide (TiO_2) is a most common photocatalyst candidate applied in H_2 production and degradation of organic pollutants in water because of its stability against photocorrosion, low-cost, and suitable bandgap with appropriate conduction band and valence band alignments [7,8]. However, the wide band gap which leads to its poor light absorption and rapid recombination of electron–hole pairs resulting in low photocatalytic activity has greatly restrict the efficiency of TiO_2 for practical applications [9,10]. Thus, considerable efforts have been made to improve TiO_2 light harvesting and facilitate the electron–hole pair separation [11-12], which involve, for instance, doping with noble metals [13-14], combining with semiconductor quantum dots (QDs) [15,16] and carbon dots (CDs) [9,17], or sensitizing with organic dyes [18]. It is also known that CuO is a superior co-catalyst suitably incorporated with TiO_2 to enhance the photocatalytic efficiency owing to its broader solar absorption range [10,19].

One-dimensional (1D) nanofibers (NFs) are ideal material for applications in electronic and optoelectronic devices due to their unique functional properties such as semi-directed charge transport, enhanced charge carrier mobility and large surface area [20-22]. The electron mobility of 1D semiconductor nanostructures is typically several orders of magnitude higher than that of corresponding spherical nanoparticles [23]. Until now, electrospinning technique for fabrication of 1D NFs has been investigated most extensively because of its high throughput under continuous process and mild conditions as well as its flexibility in controlling the fiber diameter from nanometers to a few micrometers [24]. Electrospun TiO_2-based composite NFs, including TiO_2/Au [25,26], TiO_2/Ag [26], TiO_2/N [27,28] and TiO_2/CuO [10,29] have been reported elsewhere which display photocatalytic performances both in H_2 generation and organic pollutant degradation. However, only a limited work is focused on simultaneous surface texturing, heterostructuring and structural stability of electrospun TiO_2-based composite NFs. The structural stability is derived from direct addition of co-catalyst nanoparticles for improvement of catalytic activity without detrimental migration and coalescence of the nanoparticles during long term photoreaction.

Herein, we present for the first time the fabrication of wheat grain-like textured TiO_2/CuO composite NFs *via* a simple electrospinning process. Direct amalgamation of copper nanoparticles during the electrospinning of TiO_2 NFs not only produces unique textured morphology but also achieves structural stability and enhanced catalytic activity of the NFs. The composite NFs were used for photocatalytic H_2 generation by sacrificial water splitting and pollutant degradation. The H_2 generation rate of the as-synthesized TiO_2/CuO composite NFs was 16.8 times more than that of bare TiO_2 NFs. Moreover, the TiO_2/CuO composite NFs were shown to be reusable without significant deterioration of its photocatalytic activity. These findings open up a new pathway for a scalable fabrication of low-cost and high-performance fibrous photocatalysts.

Experimental

Materials

Copper (II) sulfate pentahydrate ($CuSO_4 \cdot 5H_2O$), polyethylene glycol 8000 (PEG 8000), ascorbic acid, sodium hydroxide (NaOH), sodium borohydride ($NaBH_4$), polyvinylpyrrolidone (PVP; M_w=1,300,000), tetrabutyl titanate (TBT), methyl orange (MO), hydrogen peroxide (H_2O_2, 30%), methanol and ethanol were purchased from standard sources. All chemicals were used as received without further purification.

Synthesis of copper nanoparticles

The copper nanoparticles were synthesized according to a previous literature procedure [30,31]. In a typical run, copper solution was prepared by dissolving 0.0160 g $CuSO_4 \cdot 5H_2O$ in 10 mL of deionized water firstly. Next, 7.2 g of PEG 8000 was added to the aqueous solution containing the copper salt while vigorously stirred. Then, 0.0352 g of ascorbic acid was added to the synthesis solution. After ascorbic acid was completely dissolved, the pH value of the solution was adjusted to 12 by adding sodium hydroxide (0.1 M) solution dropwise. Finally, a 3 mL $NaBH_4$ (0.1 M) in deionized water was prepared and added under continuous rapid stirring. The color change of the solution from red to black indicated a successful reduction reaction. The mixture was further stirred rapidly for around 10 min to allow the reaction to complete. The copper nanoparticles were separated and washed with deionized water by centrifugation in order to remove excess PEG and other impurities. The resulting precipitates were dried under vacuum overnight.

Fabrication of wheat grain textured TiO_2/CuO composite NFs

TiO_2/CuO composite NFs were prepared by the electrospinning technique. Typically, 0.25 g of PVP and 0.5 g of TBT were added into the 2.5 g of ethanol solution followed by different amount of as-prepared copper nanoparticles which were dispersed by sonication for 1 h. The amount of copper nanoparticles incorporated range from 0, 0.6, 1.5, 2.5, 3.5 to 4.5 wt% copper nanoparticles, which were labeled as TC(0), TC(0.6), TC(1.5), TC(2.5), TC(3.5)and TC(4.5), respectively. The mixture was subsequently mixed for 5 h using magnetic stirrer at room temperature to obtain a homogenous and clear Cu–TBT–PVP precursor solution. Subsequently, electrospinning was carried out at an applied voltage of 18 kV and a flow rate of 4 mL h^{-1}. The distance between needle tip and aluminum foil collector was 15 cm. The collected NF mats were hydrolyzed in air for 3 h. Finally, the as-spun NFs were calcined in air at 500 °C for 2 h in a furnace, at temperature ramp rate of 2 °C min^{-1} to obtain TiO_2/CuO composite NFs. Moreover, the as-spun TC (2.5) composite NFs were calcined in air at 300, 400, 500 and 600 °C for 2 h.

Characterization of TiO_2/CuO composite NFs

The fabricated photocatalysts were analyzed using an X-ray diffractometer (XRD, Philips X-ray diffractometer with Cu Kα radiation at λ=1.541 Å) to obtain crystallographic information. Morphology and structural characteristics were studied using a field-emission scanning electron microscope (FESEM, JEOL FEG JSM 7001F) and a transmission electron microscope (TEM, Phillips FEG CM300), respectively. The elements present in the TiO_2 composites were analyzed by energy-dispersive X-ray spectroscopy (EDX, Oxford Instruments). The absorption spectra of photocatalysts were obtained using a UV-visible spectrophotometer (UV–vis, Shimadzu UV-3600). X-Ray photoelectron spectroscopy (XPS, VG Thermo Escalab 220I-XL) was employed to study the chemical composition of the photocatalyst.

Photocatalytic water splitting

5 mg of photocatalyst, 9 mL DI water and 1 mL methanol were mixed in a 25 ml quartz cylindrical reaction cell and stirred for 30 min to form a homogeneous suspension. The reactor was purged with argon (Ar) gas for 10 min prior to illumination with a 300 W xenon arc lamp of intensity 100 mW cm^{-2}. Gas samples were analyzed using a gas chromatograph (Shimadzu GC-2014AT).

Degradation of MO solution

The photocatalytic reactions of 15 ml of 20 mg mL^{-1} MO aqueous solution with extra 0.5 mL of H_2O_2 was carried out based on 5 mg of TC(0) and TC(1.5) under light irradiation with the same Xe arc lamp. The concentration of MO was analyzed using a UV–vis spectrophotometer and the maximal absorbance peak value was noted to plot the amount of MO degraded and thus, determine the photodegradation activity of the composite.

Results and discussion

The successful preparation of NFs was carried out *via* a simple electrospinning process which is regarded as a scalable approach to produce continuous fibers from sub-micron down to nanometer diameter (Figure 1a) [24]. Figure 1b shows the photograph of TC(2.5) electrospun NFs mat with an area of more than 200 cm^2 by electrospinning Cu–TBT–PVP solution for 1 h. The corresponding SEM images of the TC(2.5) electrospun NFs mat before and after annealing are shown in Figure 1c and d, respectively. The Cu–TBT–PVP NFs with average diameter of *ca.* 280 nm interweave randomly, constructing a three-dimensional (3D) porous mat. After annealing, copper nanoparticles were converted to the CuO nanoparticles and at the same time PVP was removed. The fibrous structure of TiO_2/CuO is well preserved with an average diameter slightly decreased to *ca.* 250 nm. Each fiber consists of wheat grain-like nanoparticles on the surface that are oriented along the fiber axis. The sizes of the nanoparticles are about 25–40 nm in diameter and 60–120 nm in length.

TEM was employed to gain an insight of copper nanoparticles and TiO_2/CuO NFs structure. Figure 2a shows pure copper nanoparticles that were used for compositing the electrospun NFs. The copper nanoparticles show average diameter of 20 nm. The typical TEM images of the TiO_2/CuO composite NFs were illustrated in Figure 2b and c, it can be observed that the TiO_2/CuO composite NFs have the wheat grain textured surface, which is consistent with the result of the SEM image. Figure 2d and e shows the higher resolution TEM images of middle and surface of wheat grain textured

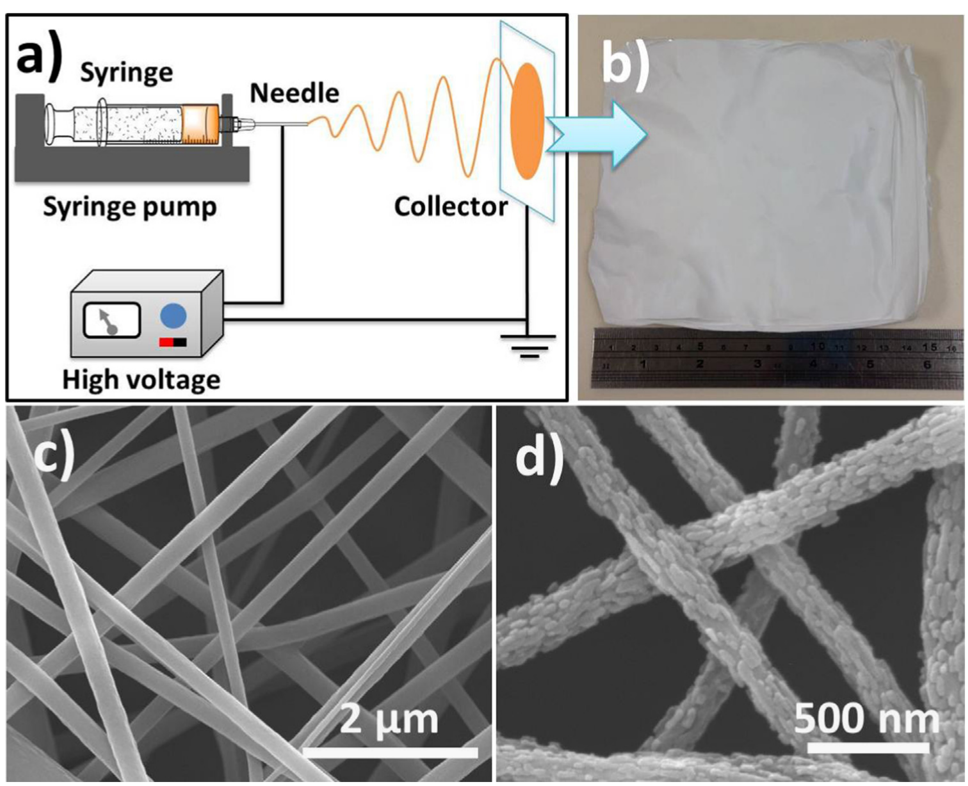

Figure 1 (a) Schematic of an electrospinning setup. (b) A digital photograph of Cu–TBT–PVP fibrous mat by electrospinning for 1 h, the content of copper nanoparticles is 2.5 wt%. The SEM images of TiO_2/CuO NFs before (c) and after (d) anneal.

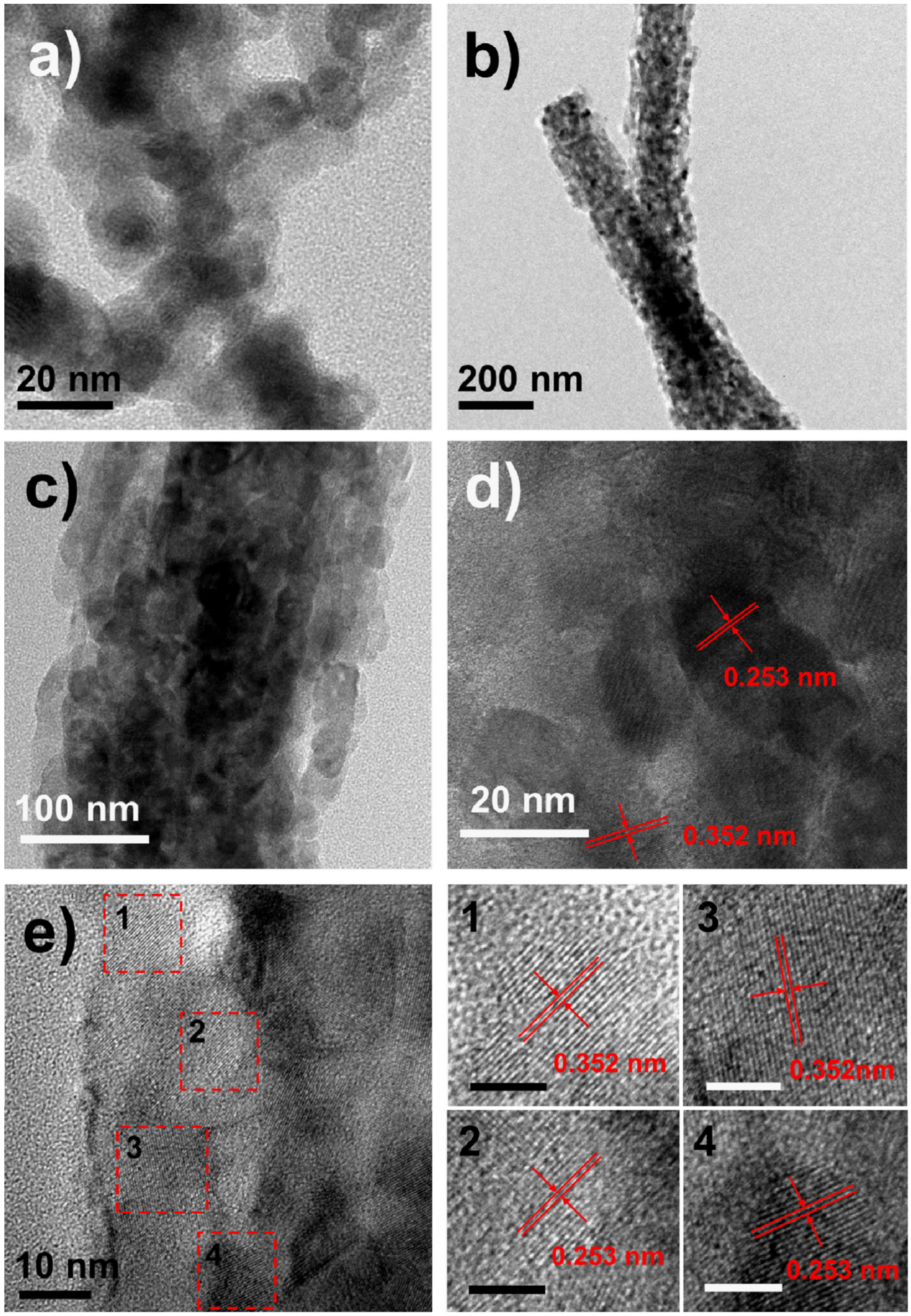

Figure 2 TEM images of (a) copper nanoparticles and TC(2.5) composite NFs at (b, c) low and (d, e) high resolution. (Section 1, 2, 3 and 4 in e, scale bar: 5 nm).

NFs. It can be seen that wheat grain textured NFs is made up of TiO_2 nanoparticles with lattice fringes of 0.352 nm attribute to the (101) plane of anatase TiO_2 (Figure 2d and e, section 1 and 3) [9,32] and CuO nanoparticles with interplanar spacing of 0.253 nm corresponds to the (111) plane of CuO (Figure 2d and Figure 2e, section 2 and 4) [10,33], which concludes that the CuO nanoparticles are homogeneously composited with TiO_2 NFs.

The crystal structures of TiO_2 and TiO_2/CuO composite NFs were also investigated by XRD and the patterns are shown in Figure 3a. The diffraction peaks in both spectra at 25.36, 37.91, 38.70, 48.15, 54.07, 55.18, 62.81, 68,84, 70.35 and 75.27^o can be indexed to the (101), (004), (112), (200), (105), (211), (204), (116), (220) and (215) crystal planes of the anatase phase of TiO_2, respectively [34]. The crystalline peak which appeared at $2\theta=35.5^o$ corresponds to the CuO crystalline structure. The corresponding EDX spectra in Figure 3b show Cu peak at 0.93 keV which indicates that the CuO nanoparticles were successfully incorporated into the TiO_2 NFs during the electrospinning process [19,35].

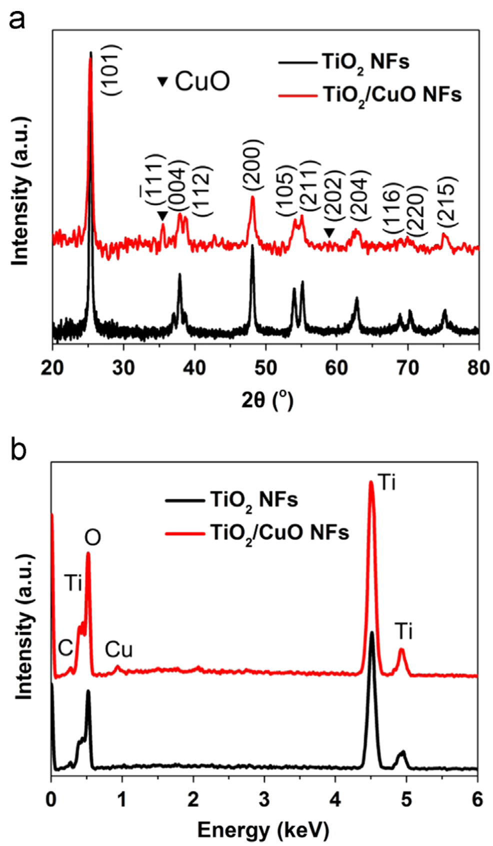

Figure 3 (a) XRD and (b) EDX spectra of TiO_2/CuO composite NFs.

The XPS analysis was employed to determine the chemical states of the TiO_2/CuO NFs, in particular Ti and Cu. The wide scan spectrum in Figure 4a shows the binding energy peaks at 285.4, 458.0, 529.9 and 933.4 eV, which are attributed to C 1s, Ti 2p, O 1s and Cu 2p, respectively. Binding energies of 458.6 and 464.5 eV are indicative of Ti $2p_{3/2}$ and Ti $2p_{1/2}$ in the high resolution Ti 2p spectra (Figure 4b) which correspond to Ti^{4+} in a tetragonal structure [10]. Meanwhile, the peak at 530.3 eV is an evidence of O 1s in TiO_2 and CuO or Cu_2O (Figure 4c). The Cu 2p peak of the TiO_2/CuO NFs is shown in Figure 4d. The Cu $2p_{3/2}$ is allocated at 934.5 eV with a shakeup satellite peak at about 943.9 eV and Cu $2p_{1/2}$ lies at 954.1 eV with a satellite peak at about 962.2 eV, which is consistent with earlier reports. The presence of shakeup satellite features for Cu 2p rules out the possibility of Cu_2O phase presence. The gap between Cu $2p_{1/2}$ and Cu $2p_{3/2}$ is about 20 eV, which is in agreement with the standard CuO spectrum [36,37].

To further optimize the performance of TiO_2/CuO NFs, we also investigated the influence of compositing with different amount of copper nanoparticles. Figure 5 depicts the SEM images of as-spun TiO_2/CuO composite NFs with various copper nanoparticles content in the precursor solution (0, 0.6, 1.5, 2.5, 3.5 and 4.5 wt%). Like most bare TiO_2 NFs, TC (0) has a rough and porous surface (Figure 5a) [34,38]. After incorporation of copper nanoparticles, TC(0.6), TC(1.5), TC (2.5), TC(3.5) and TC(4.5) have similar morphology (Figure 5b–f) with wheat grain-like texture. The average diameter of the resultant TiO_2/CuO NFs shows no apparent change, which suggests that the amount of copper nanoparticles added does not affect the diameter of the NFs.

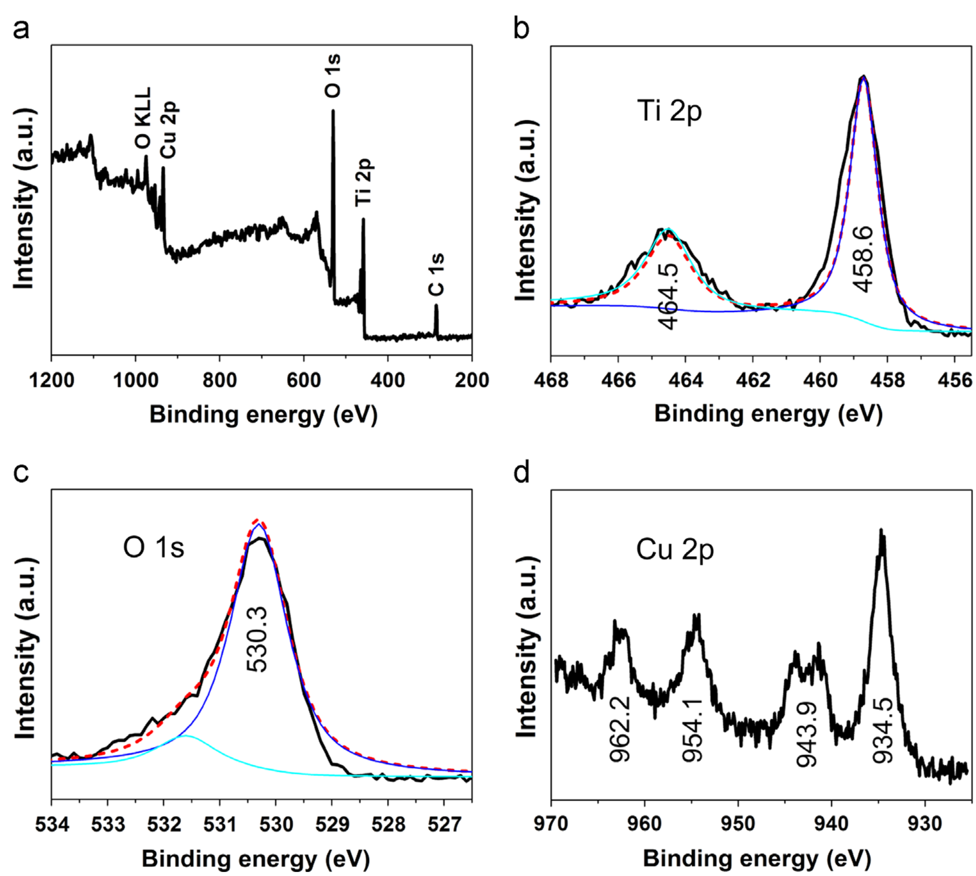

Figure 4 (a) XPS spectrum of TC(2.5) NFs; high resolution XPS spectra of TC(2.5) for NFs for (b) Ti 2p, (c) O 1s and (d) Cu 2p.

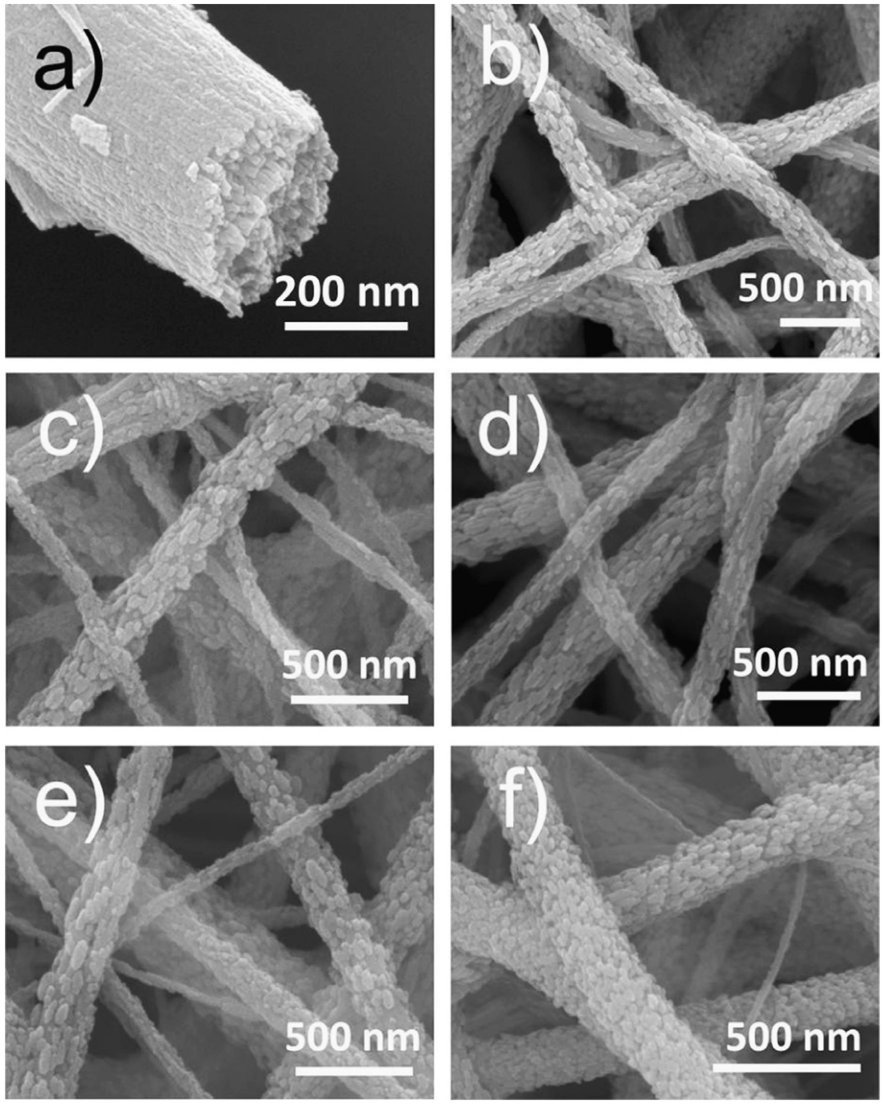

Figure 5 The SEM images for (a) TC(0), (b) TC(0.6), (c) TC(1.5), (d) TC(2.5), (e) TC(3.5) and (f) TC(4.5) NFs.

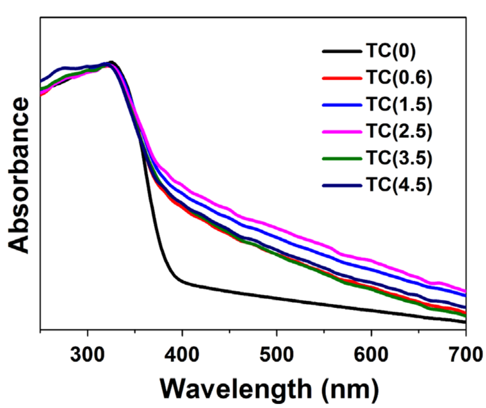

Figure 6 The UV-vis spectra of TC(0), TC(0.6), TC(1.5), TC (2.5), TC(3.5) and TC(4.5) NFs.

The corresponding UV-vis absorption measurements of TiO_2/CuO NFs were carried out and absorption spectra are shown in Figure 6. In general, the absorbance intensities increase with the addition of copper nanoparticles while the bare TiO_2 NFs exhibits the lowest intensity. The absorbance of TC(2.5) is the highest among the five TiO_2/CuO NFs samples. The absorbance of the composite NFs extends to the visible-light region, which may be beneficial for photocatalytic performance [10].

When the concentration of copper nanoparticles is fixed at 2.5 wt%, the effect of annealing temperature on the morphology of the composite NFs was studied. Figure 7a-d shows SEM images of TiO_2/CuO NFs annealed at 300, 400, 500 and 600 °C, respectively. At low temperature, it can be observed that rough surface was observed instead of wheat grain-like structure, (Figure 7a), which may attribute to the residue of the PVP. When the annealing temperature is increased to 400 °C, sparsely distributed nanoparticles are clearly observed at the surface of the NFs (Figure 7b). After annealing at 500 °C, wheat grain-like texture surface are formed (Figure 7c). As the thermal treatment temperature increases to 600 °C, the elongated wheat grain-like structures were transformed into quasi-spherical nanoparticles textured surface.

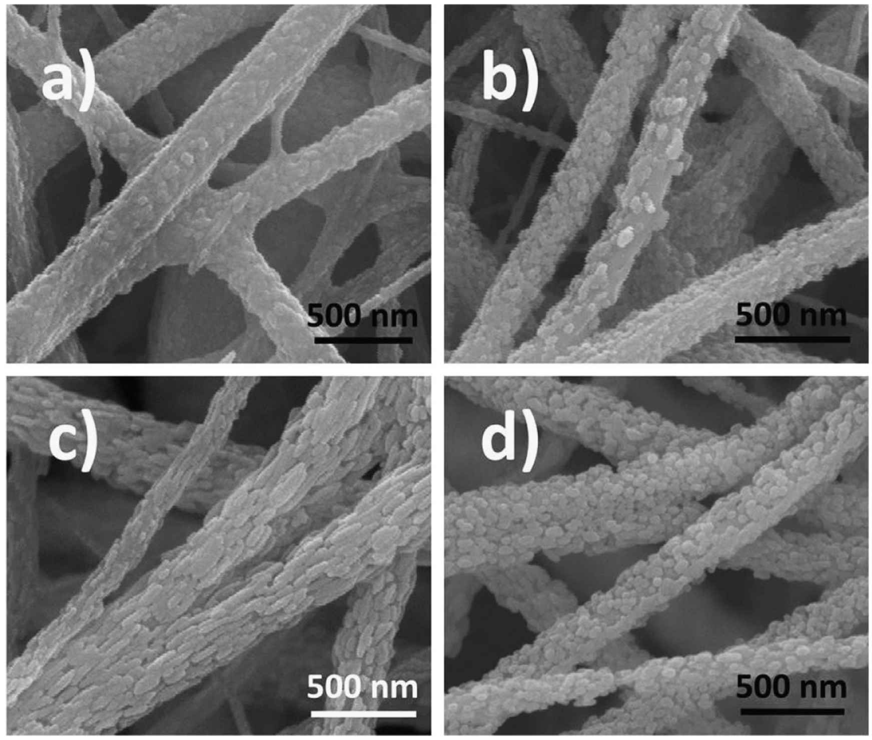

Figure 7 The SEM images for TiO_2/CuO NFs annealed under the different temperature: (a) 300, (b) 400, (c) 500 and (d) 600 °C.

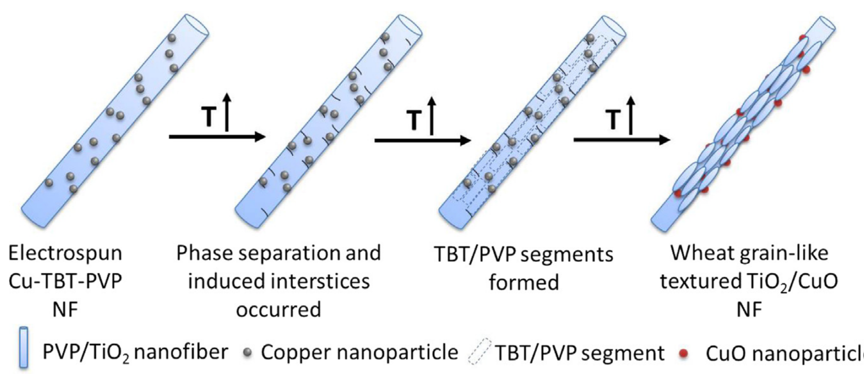

Scheme 1 Possible formation mechanism of wheat grain-like textured TiO_2/CuO NFs. .

On the basis of the aforementioned observations, a possible formation mechanism of wheat grain-like textured TiO_2/CuO NFs is proposed as follows (Scheme 1): At first, composite NFs with copper nanoparticles dispersed on TBT-PVP are obtained through electrospinning. Phase separation occurred between TBT, copper nanoparticles and polymer matrices. Subsequently, when the PVP phase was removed by calcination, interstices may be induced at the interface of TBT and copper phases such that the fiber may be segregated into TBT/PVP segments. With further PVP elimination, the TBT/PVP segments were converted into elongated nanoparticles with wheat grain-like morphology. Meanwhile, the evaporation and separation of PVP and TBT phases promote self-orientation of wheat grain-like nanoparticles along fiber axis [34]. Also, at lower annealing temperature, the elongated wheat grain particles consist of smaller TiO_2 crystallites grain size which possess high surface energy that facilitate the aggregation of the crystallites. In contrast, at higher annealing temperature, the grain size of the TiO_2 crystallites will increase which may lead to formation of individual particles [10,39,40]. Furthermore, high thermal treatment promotes rounding of these crystallites into quasi-spherical shape.

To determine the photocatalytic activity of these as-fabricated NFs, we utilized them for hydrogen production from photocatalytic water splitting [9,41]. In this case, we found that the H_2 evolution rate can be immensely enhanced by introducing copper nanoparticles into the bare TiO_2 NFs and optimizing its performance by tuning the amount of CuO composited. Figure 8a and b illustrates the time course of H_2 production of the TiO_2 NFs and TiO_2/CuO composite NFs obtained from different copper amounts which have been annealed at 500 °C. Bare TiO_2 NFs (TC (0)) which is used as the control sample show H_2 evolution

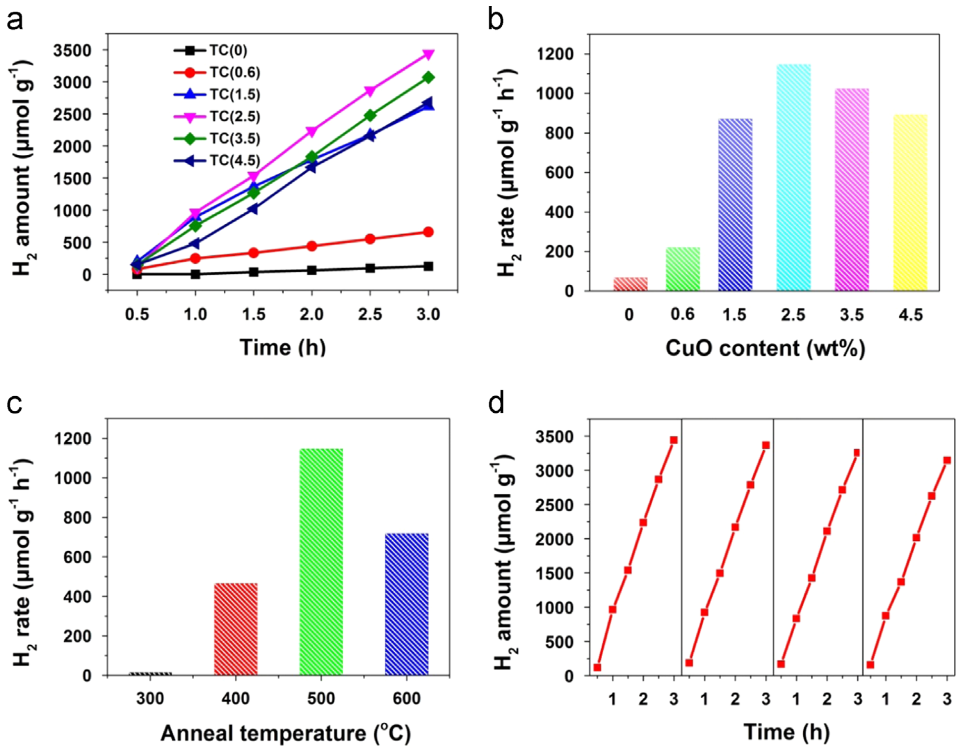

Figure 8 (a) H_2 amount over the irradiation time and (b) H_2 rates for the TC(0), TC(0.6), TC(1.5), TC(2.5), TC(3.5) and TC(4.5) NFs. (b) Photocatalytic H_2 production studies of TiO_2/CuO annealed at different temperature (300, 400, 500 and 600 °C). (d) A typical time course of H_2 production from TC(2.5) for 4 cycles.

rate of about 68.3 μmol g^{-1} h^{-1}(black line), while the amount of H_2 evolved increases with CuO content up to 2.5 wt%. The highest H_2 evolution rate of 1146.9 μmol g^{-1} h^{-1} occurred with TC(2.5) (pink line), which is 16.8 times higher than that of bare TiO_2 NFs. Furthermore, the H_2 generation rates of TiO_2/CuO composite NFs annealed at different temperatures (300, 400, 500 and 600 °C; copper nanoparticle content of 2.5 wt%) were also studied (Figure 8c). The sample annealed at 500 °C shows the highest evolution rate among them possibly due to its optimal crystallinity for improved charge transfer [10,42]. Under lower temperature, we believe, the crystallinity of TiO_2 is lower and supporting polymer material PVP is not removed completely. Whereas, the higher temperature may lead to higher degree of crystallinity with larger crystal size and crystal phases transformation [39,40], hence decreasing the rate of H_2 evolution [10,38]. To determine the reusability of photocatalyst, water splitting by TC(2.5) was carried out for another three cycles. As shown in Figure 8d, no obvious loss of photocatalytic performance was observed, suggesting that the composite NFs are structurally stable. An energy level diagram showing the positions of the bands of TiO_2 and CuO is presented in Scheme 2. Absorption of light greater than the band-gap energy of TiO_2 generates electrons and holes in the CB and VB respectively. The sacrificial electron donor consumes holes in the VB rapidly leaving electrons in the CB of TiO_2. The CB position of CuO below the CB of TiO_2 permits the transfer of electrons from the CB of TiO_2 to the CB of CuO, where is served as the reduction sites for H_2 production [10,19].

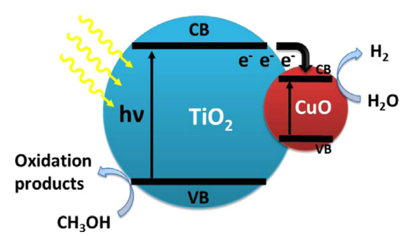

Scheme 2 Schematic diagram of the photocatalytic H_2 generation over the TiO_2/CuO heterojunctions.

Finally, the photocatalytic performance was tested *via* photocatalytic degradation of MO, a common textile pollutant [8,43]. Figure 9a exhibits the content changes of MO in the absence and in the presence of different composites. A control experiment was carried out to show that photodegradation is not apparent without the use of a nanocomposite photocatalyst. Also, in order to compensate for the lack of oxygen caused either by consumption or slow oxygen mass transfer, inorganic oxidants H_2O_2 [44,45] was added into the degradation solution. H_2O_2 has a positive effect on the rate of the photocatalytic oxidation of organic molecules in water by avoiding electron/hole recombination, as they act as electron acceptors. This results in full degradation of the MO dye after 120 min. In contrast, degradation capabilities of bare TiO_2 NFs and TiO_2/CuO composite NFs were tested and shown to degrade the MO molecules after 70 and 60 min of UV–vis irradiation, respectively. TiO_2/CuO composite NFs display a higher photocatalytic activity in MO degradation. The degradation of MO dye is approximately

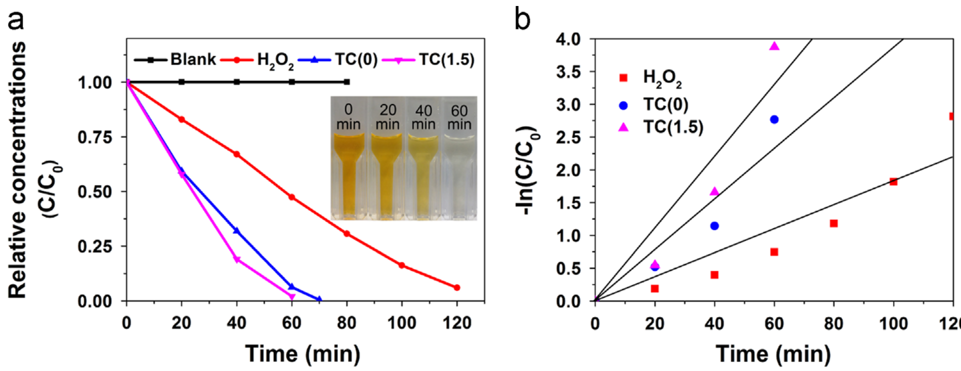

Figure 9 (a) Degradation kinetics and (b) pseudo-first order kinetics of time evolution MO photodegradation study in absence and presence of various photocatalysts. Inset: Digital photographs illustrating time MO photodegradation using TC(1.5).

33.1, 68.2 and 81.1% for H_2O_2, bare TiO_2 and TiO_2/CuO NFs respectively after photo-irradiation for 40 min. A digital photograph illustrating the time evolution photodegradation study using TC(1.5) is shown in Figure 9a(inset). Figure 9b shows the pseudo-first order kinetics of the MO degradation of the various photocatalysts. The efficiency of MO photodegradation by the composite was determined quantitatively using the pseudo-first order model [46] as follows:

$$\ln(C_0/C_t) = kt$$

where C_0 and C_t are the concentrations of dye at time 0 and t, respectively and k is the pseudo-first order rate constant. The constants k of the bare TiO_2 and TiO_2/CuO NFs photocatalysts are 0.0388 and 0.0571 min^{-1}, respectively. The results clearly demonstrate that the composites exhibit enhanced photodegradation over bare TiO_2 NFs.

Conclusion

In summary, TiO_2/CuO composite NFs with novel wheat grain texture have been successfully fabricated *via* electrospinning. Phase separation and evaporation have induced orientation of the wheat grain-like nanoparticles along the axial direction of the resulting TiO_2/CuO NFs. Different copper contents and annealing temperatures have been explored for H_2 generation from photocatalytic water splitting. The NFs obtained at 500 °C for 2 h with the copper content of 2.5 wt% shows the highest H_2 generation rate of 1146.9 μmol $g^{-1} h^{-1}$, which is much higher than that of bare TiO_2 NFs. In addition, TiO_2/CuO composite NFs have favorable capability for photodegradation of organic pollutant in water. Therefore, this simple and continuous synthetic approach may offer an avenue for preparation of the fibrous photocatalyst mat with the different morphology and improved physicochemical properties for vast environmental and energy applications.

Acknowledgments

This work is supported by A*star R-263-000-A96-305 and MOE R-144-000-325-112.

References

[1] K. Maeda, K. Teramura, D.L. Lu, T. Takata, N. Saito, Y. Inoue, K. Domen, Nature 440 (2006) 295.
[2] P.J. Dauenhauer, J.R. Salge, L.D. Schmidt, J. Catal. 244 (2006) 238-247.
[3] D. Voiry, H. Yamaguchi, J.W. Li, R. Silva, D.C.B. Alves, T. Fujita, M.W. Chen, T. Asefa, V.B. Shenoy, G. Eda, M. Chhowalla, Nat. Mater. 12 (2013) 850-855.
[4] I.K. Kapdan, F. Kargi, Enzyme Microb. Technol. 38 (2006) 569-582.
[5] J.R. Benemann, N.M. Weare, Science 184 (1974) 174-175.
[6] X.R. Cao, G.H. Tian, Y.J. Chen, J. Zhou, W. Zhou, C.G. Tian, H.G. Fu, J. Mater. Chem. A 2 (2014) 4366-4374.
[7] T. Kawai, T. Sakata, Nature 282 (1979) 283-284.
[8] W.L. Ong, M. Gao, G.W. Ho, Nanoscale 5 (2013) 11283-11290.
[9] J. Wang, M. Gao, G.W. Ho, J. Mater. Chem. A 2 (2014) 5703-5709.
[10] S.S. Lee, H.W. Bai, Z.Y. Liu, D.D. Sun, Appl. Catal. B: Environ. 140-141 (2013) 68-81.
[11] M.Y. Wang, J. Ioccozia, L. Sun, C.J. Lin, Z.Q. Lin, Energy Environ. Sci. 7 (2014) 2182-2202.
[12] M.Y. Wang, L. Sun, Z.Q. Lin, J.H. Cai, K.P. Xie, C.J. Lin, Energy Environ. Sci. 6 (2013) 1211-1220.
[13] D. D'Elia, C. Beauger, J.F. Hochepied, A. Rigacci, M.H. Berger, N. Keller, V. Keller-Spitzer, Y. Suzuki, J.C. Valmalette, M. Benabdesselam, P. Achard, Int. J. Hydrog. Energy 36 (2011) 14360-14373.
[14] M. Murdoch, G.I.N. Waterhouse, M.A. Nadeem, J.B. Metson, M.A. Keane, R.F. Howe, J. Llorca, H. Idriss, Nat. Chem. 3 (2011) 489-492.
[15] Y.L. Lee, C.F. Chi, S.Y. Liau, Chem. Mater. 22 (2010) 922-927.
[16] M.D. Ye, J.J. Gong, Y.K. Lai, C.J. Lin, Z.Q. Lin, J. Am. Chem. Soc. 134 (2012) 15720-15723.
[17] H.J. Yu, Y.F. Zhao, C. Zhou, L. Shang, Y. Peng, Y.H. Cao, L.Z. Wu, C.H. Tung, T.R. Zhang, J. Mater. Chem. A 2 (2014) 3344-3351.
[18] W.J. Youngblood, S.H.A. Lee, K. Maeda, T.E. Mallouk, Acc. Chem. Res. 42 (2009) 1966-1973.
[19] J. Bandara, C.P.K. Udawatta, C.S.K. Rajapakse, Photochem. Photobiol. Sci. (2005)857-861.
[20] H. Wu, L.B. Hu, M.W. Rowell, D.S. Kong, J.J. Cha, J.R. McDonough, J. Zhu, Y. Yang, M.D. McGehee, Y. Cui, Nano Lett. 10 (2010) 4242-4248.
[21] H. Wu, D.S. Kong, Z.C. Ruan, P.C. Hsu, S. Wang, Z.F. Yu, T.J. Carney, L.B. Hu, S.H. Fan, Y. Cui, Nat. Nanotechnol. 8 (2013) 421-425.
[22] V.T. Le, H. Kim, A. Ghosh, J. Kim, J. Chang, Q.A. Vu, D.T. Pham, J.H. Lee, S.W. Kim, Y.H. Lee, ACS Nano 7 (2013) 5940-5947.

[23] C.L. Zhang and S.H. Yu, Chem. Soc. Rev. 13 (2014) 4423–4448.
[24] A. Greiner, J.H. Wendorff, Angew. Chem. Int. Ed. 46 (2007) 5670–5703.
[25] A.A. Madhavan, G.G. Kumar, S. Kalluri, J. Joseph, S. Nagarajan, S. Nair, K.R.V. Subramanian, A. Balakrishnan, J. Nanosci. Nanotechnol. 12 (2012) 7963–7967.
[26] S.H. Nam, H.S. Shim, Y.S. Kim, M.A. Dar, J.G. Kim, W.B. Kim, ACS Appl. Mater. Interfaces 2 (2010) 2046–2052.
[27] H.P. Li, W. Zhang, S.Y. Huang, W. Pan, Nanoscale 4 (2012) 801–806.
[28] V.J. Babu, M.K. Kumar, A.S. Nair, T.L. Kheng, S. I. Allakhverdiev, S. Ramakrishna, Int. J. Hydrog. Energy 37 (2012) 8897–8904.
[29] S.S. Lee, H.W. Bai, Z.Y. Liu, D.D. Sun, Water Res. 47 (2013) 4059–4073.
[30] T.M.D. Dang, T.T.T. Le, E. Fribourg-Blanc, M.C. Dang, Adv. Nat. Sci.: Nanosci. Nanotechnol. 2 (2011) 025004.
[31] T.M.D. Dang, T.T.T. Le, E. Fribourg-Blanc, M.C. Dang, Adv. Nat. Sci.: Nanosci. Nanotechnol. 2 (2011) 015009.
[32] W.Q. Wu, H.S. Rao, Y.F. Xu, Y.F. Wang, C.Y. Su, D.B. Kang, Sci. Rep. 3 (2013) 1892.
[33] Q.B. Zhang, D.G. Xu, T.F. Hung, K.L. Zhang, Nanotechnology 24 (2013) 065602.
[34] L.F. Wang, Y. Zhao, J.M. Wang, X. Hong, J. Zhai, L. Jiang, F.S. Wang, Appl. Surf. Sci. 255 (2009) 4944–4949.
[35] N.T. Ly, T.V. Hoang, T.H.L. Ngo, V.C. Nguyen, D.T. Tran, H.M. Do, D.L. Vu, X.N. Nguyen, T.H. Dao, Q.H. Le, M.H. Nguyen, V.H. Le, Adv. Nat. Sci.: Nanosci. Nanotechnol. 3 (2012) 045009.
[36] M.A. Dar, S.H. Nam, Y.S. Kim, W.B. Kim, J. Solid State Electrochem. 14 (2010) 1719–1726.
[37] D. Tahir, S. Tougaard, J. Phys.: Condens. Matter 24 (2012) 175002.
[38] S. Chuangchote, J. Jitputti, T. Sagawa, S. Yoshikawa, ACS Appl. Mater. Interfaces 1 (2009) 1140–1143.
[39] A.K. Srivastava, M. Deepa, S. Bhandari, H. Fuess, Nanoscale Res. Lett. 4 (2009) 54–62.
[40] W. Li, C. Ni, H. Lin, C.P. Huang, S. Ismat Shah, J. Appl. Phys. 96 (2004) 6663–6668.
[41] M. Gao, C.K.N. Peh, W.L. Ong, G.W. Ho, RSC Adv. 3 (2013) 13169–13177.
[42] J.H. Pan, H. Dou, Z. Xiong, C. Xu, J. Ma, X.S. Zhao, J. Mater. Chem. 20 (2010) 4512–4528.
[43] W.L. Ong, S. Natarajan, B. Kloostra, G.W. Ho, Nanoscale 5 (2013) 5568–5575.
[44] C.G. Silva, J.L. Faria, J. Mol. Catal. A: Chem. 305 (2009) 147–154.
[45] M.M. Cheng, W.H. Ma, J. Li, Y.P. Huang, J.C. Zhao, Environ. Sci. Technol. 38 (2004) 1569–1575.
[46] J.M. Herrmann, H. Ahiri, Y. Ait-Ichou, G. Lassaletta, A.R. Gonzalez-Elipe, A. Fernandez, Appl. Catal., B: Environ. 13 (1997) 219–228.

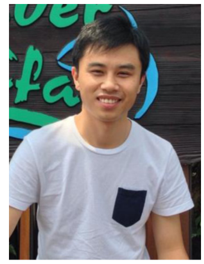

Liangliang Zhu received his Ph.D. degree in Material Chemical Engineering at Nanjing University of Technology, China in 2013. He is now a research fellow at the Department of Electrical & Computer Engineering at National University of Singapore (NUS). His current research interest is preparation of photocatalysts for hydrogen production and photodegradation.

Prof. Minghui Hong received his Ph.D. degree in laser ablation and real-time monitoring in 2000. Currently, he is a Professor in Department of Electrical & Computer Engineering at National University of Singapore (NUS) and a Senior Scientist at Data Storage Institute, A*STAR. His research interests include laser ablation, optical signal diagnostics/process real time monitoring and its industrial applications on laser micro-processing and nano-engineering.

Prof. Ghim Wei Ho received her Ph.D. on semiconductor nanostructures at the Nanoscience Centre, University of Cambridge in 2006. She is an Associate Professor of the Department of Electrical & Computer Engineering at the National University of Singapore (NUS). She is also one of the pioneer associates of the Engineering Science Programme (ESP) at NUS. Her research thrusts are centred around the development of nanostructured materials for photovoltaic applications and nanomaterials for photocatalytic applications.